 FDMP, vol.6, no.4, pp.369-384, 2010

Marangoni-Natural Convection in Liquid Metals in the Presence of a Tilted Magnetic Field

S. Hamimid[1] **and A. Amroune**[1]

Abstract: The Navier–Stokes and energy equations are numerically solved to investigate two-dimensional convection (originating from the combined effect of buoyancy and surface tension forces) in a liquid metal subjected to transverse magnetic fields. In particular, a laterally heated horizontal cavity with aspect ratio (height/width) =1 and Pr=0.015 is considered (typically associated with the horizontal Bridgman crystal growth process and commonly used for benchmarking purposes). The effect of a uniform magnetic field with different magnitudes and orientations on the stability of the two distinct convective solution branches (with a single-cell or two-cell pattern) of the steady-state flows is investigated. The effects induced by increasing values of the Rayleigh and Hartmann numbers on the heat transfer rate are also discussed.

Keywords: Numerical modeling, semiconductor melt, magnetic field suppression, thermocapillary convection, solidification.

Nomenclature

$\overrightarrow{B}$	Uniform magnetic field, $B_x\overrightarrow{ex}+B_y\overrightarrow{ey}$ $[T]$
B_x, B_y	Space independent components of B of constant $[T]$
B_0	Magnitude of $\overrightarrow{B}$ $[T]$
Cp	Specific heat at constant pressure $[J.kg^{-1}.k^{-1}]$
g	Gravitational acceleration $[m.s^{-2}]$
Ha	Hartmann number $=B_0L/(\sigma_e\rho\nu)^{1/2}$
H	Enclosure height $[m]$
k	Effective thermal conductivity $w.m^{-1}.k^{-1}$
Ma	Marangoni number $=\gamma\Delta T/\mu\alpha$
Nu	Nusselt number
Nu_{avg}	Average Nusselt number
P	Fluid pressure $[Pa]$

[1] UMBB, Boumerdes, ALGERIA.

Pr	Prandtl number $=\nu/\alpha$
Ra	Rayleigh number $=\frac{g\beta\Delta TL^3}{\nu\alpha}$
t	Time $[s]$
T	Temperature $[K]$
T_0	Reference temperature $=\frac{T_C-T_H}{2}$ $[K]$
u	Velocity in x-direction $[m.s^{-1}]$
v	Velocity in y-direction $[m.s^{-1}]$
$\overrightarrow{V}$	Field velocity $(u\overrightarrow{ex}+v\overrightarrow{ey})$ $[m.s^{-1}]$
x,y	Cartesian coordinates $[m]$
X,Y	Dimensionless coordinates

Greek symbols

α	Thermal diffusivity $[m^2.s^{-1}]$
β	Coefficient of thermal expansion of fluid. $[k^{-1}]$
ρ	Fluid density at reference temperature (T_0)
σ	Surface tension $[N.m^{-1}]$
σ_e	Electrical conductivity $[S.m^{-1}]$
μ	Effective dynamic viscosity $[Kg.m^{-1}.s^{-1}]$
ν	Effective kinematic viscosity $[m^2.s^{-1}]$
γ	Temperature coefficient of the surface Tension $[N.m^{-1}.K^{-1}]$
ΔT	Difference in temperature = $[T_C - T_F\ K]$
Ψ	Streamfunction $[m^2.s^{-1}]$
θ	Dimensionless temperature $=\frac{T-T_0}{\Delta T}$.
φ	The orientation of the magnetic field with horizontal axis $[^\circ]$
τ	Dimensionless time

Subscripts

max	Maximum value
min	Minimum value
avg	Average value
0	Reference state
C	Cold
H	Hot

1 Introduction

When a free surface is present in free convection liquid flow, the variation in the surface tension at the free surface due to temperature gradients can induce motion within the fluid. Such flow is known either as thermocapillary flow or Marangoni convection.

Thermocapillary convection is of importance in a wide variety of materials processes associated with unbalanced surface tension, in particular, benefiting; from the reduction of buoyancy convection and hydrostatic pressure in low gravity.

Marangoni convective flows are encountered in many technological processes involving free surfaces of a liquid with a nonuniform temperature distribution. Widespread interest in these flows is related with manufacturing of semiconductor monocrystals in a microgravity environment [Ostrach (1982) and Favier (1990)].

Hadid and Roux (1990) investigated numerically the influence of thermocapillary forces on natural convection flow in a shallow cavity. Numerous studies have been already devoted to the numerical modeling of buoyancy flows in cavities [e.g., Achoubir et al. (2008), Bucchignani (2009), Djebali et al. (2009), Mezrhab and Naji (2009)] and to the electromagnetic stabilization of the convective flows in several different configurations [e.g., Weiss (1981), Ben Hadid and Henry (1997)].

Such magnetoconvective flows in bounded domains have been solved through two- and three-dimensional numerical simulations by several researchers in recent years [Ozoe and Maruo (1987); Ozoe and Okada (1989); Armour and Dost (2009); Mechighel et al. (2009)].

Rudraiah and Venkatachalappa (1995), in particular, investigated the effect of surface tension gradients on buoyancy driven flow of an electrically conducting fluid in a square cavity in the presence of a vertical transverse magnetic field. The purpose of the investigation was to see how this force damps hydrodynamic movements (since, this is required to enhance crystal purity, increase compositional uniformity and reduce defect density).

In the present investigation, we have considered the problem of combined buoyancy and thermocapillary convection flow of an electrically conducting fluid within a square enclosure under an externally imposed constant uniform magnetic field. We have chosen a fluid that is characterized by a small Prandtl number (Pr = 0.015, which is appropriate for liquid metal and semi-conductor melts, (Tab. 1)) and a Marangoni number (Ma =1000). The transport equations describing the momentum and heat transfer have been discretized using the finite volume method (FVM) with staggered grids. Solutions of the problem in terms of streamlines, isotherms as well as heat transfer rate from the heated surface have been obtained for values of the Rayleigh number, Ra, equal to 10^4, 10^5 and 10^6, the Hartmann number, Ha, which

depends on the transverse magnetic field magnitude, ranging from 0.0 to 150.

Table 1: Physical properties of silicon melt

Melting point temperature $T_m\,[K]$	1685
Density$\rho\,\left[g/cm^3\right]$	2.42
Thermal diffusivity $\alpha\,\left[cm^2/s\right]$	2.44×10^{-1}
Kinematic viscosity $\nu\,\left[cm^2/s\right]$	2.45×10^{-3}
Prandtl number	0.015
Thermal conductivity $\lambda\,[w/cmk]$	0.64
Surface tension $\sigma\,[dyne/cm]$	7.33×10^{2}

2 Mathematical model and analysis

The liquid is assumed as a Newtonian fluid filling a square enclosure as shown in Fig. 1. The right and the left walls are maintained at uniform temperatures T_H and T_C, respectively, and are such that $T_H \succ T_C$. The upper and lower boundaries are considered to be adiabatic.

We further assume that the cavity is permeated by a uniform magnetic field

$$\overrightarrow{B} = B_x\overrightarrow{ex} + B_y\overrightarrow{ey} \tag{1}$$

The free surface is idealized as non-deformable and adiabatic from the environmental gas. The surface tension is considered to be a linearly decreasing function of the temperature, as:

$$\sigma(T) = \sigma(T_0) - \gamma(T - T_0) \tag{2}$$

Fluid flow in the system is described by the Navier–Stokes equation (continuity and momentum equations). Assuming incompressible flow, the equation of continuity can be expressed as

$$\frac{\partial U}{\partial X} + \frac{\partial V}{\partial Y} = 0 \tag{3}$$

Using the Boussinesq approximation, the Navier–Stokes equations for momentum for an unsteady laminar flow can be written as

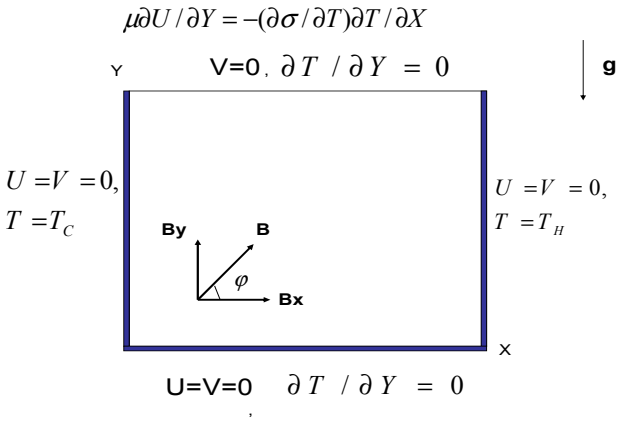

Figure 1: The flow configuration and coordinate system.

$$\frac{\partial U}{\partial \tau}+U\frac{\partial U}{\partial X}+V\frac{\partial U}{\partial Y}=-\frac{\partial P}{\partial X}+\Pr(\frac{\partial^2 U}{\partial X^2}+\frac{\partial^2 U}{\partial Y^2})+\Pr Ha^2(V\sin\varphi\cos\varphi-U\sin^2\varphi) \tag{4}$$

$$\frac{\partial V}{\partial \tau}+U\frac{\partial V}{\partial X}+V\frac{\partial V}{\partial Y}=-\frac{\partial P}{\partial Y}+\Pr(\frac{\partial^2 V}{\partial X^2}+\frac{\partial^2 V}{\partial Y^2})+Ra\Pr\theta+\Pr Ha^2(U\sin\phi\cos\phi-V\cos^2\phi) \tag{5}$$

Assuming negligible viscous heat dissipation, the differential thermal energy balance equation may be expressed as

$$\frac{\partial \theta}{\partial \tau}+U\frac{\partial \theta}{\partial X}+V\frac{\partial \theta}{\partial Y}=(\frac{\partial^2 \theta}{\partial X^2}+\frac{\partial^2 \theta}{\partial Y^2}) \tag{6}$$

The effect of the induced electric current on the external magnetic field and the Joule heating are neglected in the formulation (2)–(6). This is justified by the estimation of non-dimensional parameters characteristic for liquid metals and semiconductors (some details are given in Ref. [Gelfgat and Bar-Yoseph (2001)]).

The dimensionless initial and boundary conditions are:

$U=V=\theta=0$ for $\tau=0$

$U=V=0$, $\theta=\theta_H=0.5$ for $0\le Y\le 1$ at $X=1$

$U=V=0$, $\theta=\theta_C=-0.5$ for $0\le Y\le 1$ at $X=0$

$U=V=0$, $\frac{\partial\theta}{\partial Y}=0$ for $0\le X\le 1$ at $Y=0$

$V = 0$, $\frac{\partial \theta}{\partial Y} = 0$, $\frac{\partial U}{\partial Y} = Ma\frac{\partial \theta}{\partial X}$ for $0 \leq X \leq 1$ at $Y = 1$

In the above equationsRa, Pr, Ha and Ma are, respectively, the Rayleigh number, Prandtl number, Hartmann number and the Marangoni number which are defined as follows:

$$Ra = \frac{g\beta\Delta TL^3}{\nu^2}, \quad \Pr = \frac{\nu}{\alpha}, \quad Ha = B_0 L(\sigma_e/\rho\nu)^{1/2}, \quad Ma = \frac{\gamma\Delta TL}{\mu\alpha}.$$

The non-dimensional heat transfer rate in terms of local Nusselt number, Nu, from the right vertical heated surface is given by

$$Nu(Y) = -\frac{\partial \theta(X,Y)}{\partial X}\bigg|_{X=1} \tag{7}$$

The corresponding value of the average Nusselt number, denoted by Nu_{av}, may be calculated from the following relation

$$Nu_{av} = \int_0^1 Nu(y)dy = -\int_0^1 \left(\frac{\partial \theta(x,y)}{\partial x}\right)dy \tag{8}$$

3 Numerical solution methodology

The governing equations are discretized using the control volume approach of Patankar. In addition, the power law formulation is employed to determine the combined advective and diffusive fluxes across the boundaries of each control volume.

The unsteady term is treated with backward difference. The buoyancy and Lorentz forces in the x and y-momentum equations are treated as source terms. The conventional staggered grid system used originally in the SIMPLE scheme is adopted. The discretized equations are solved iteratively with the line-by-line procedure of tri-diagonal matrix algorithm. In this study, no uniform mesh sizes are used and 140 X 140 grids are chosen for the grid arrangement and it is found that this grid solution is enough.

4 Results and discussion

Numerical results are presented in order to determine the effects of the presence of a magnetic field, buoyancy and thermocapillary forces on the natural convection flow of an electrically conducting fluid in a square cavity. Values of the magnetic field parameter Ha range between 0 to 250, the Rayleigh numberRa, between 0 and 10^5 but for the Marangoni number, Ma, equal to 1000. Typical

value of direction of the external magnetic field with the horizontal considered to be $\varphi = 0, \pi/6, \pi/4, \pi/3, \pi/2, 4\pi/6, 5\pi/6, \pi, 7\pi/6, 8\pi/6, 9\pi/6, 10\pi/6, 11\pi/6$ and 2π.

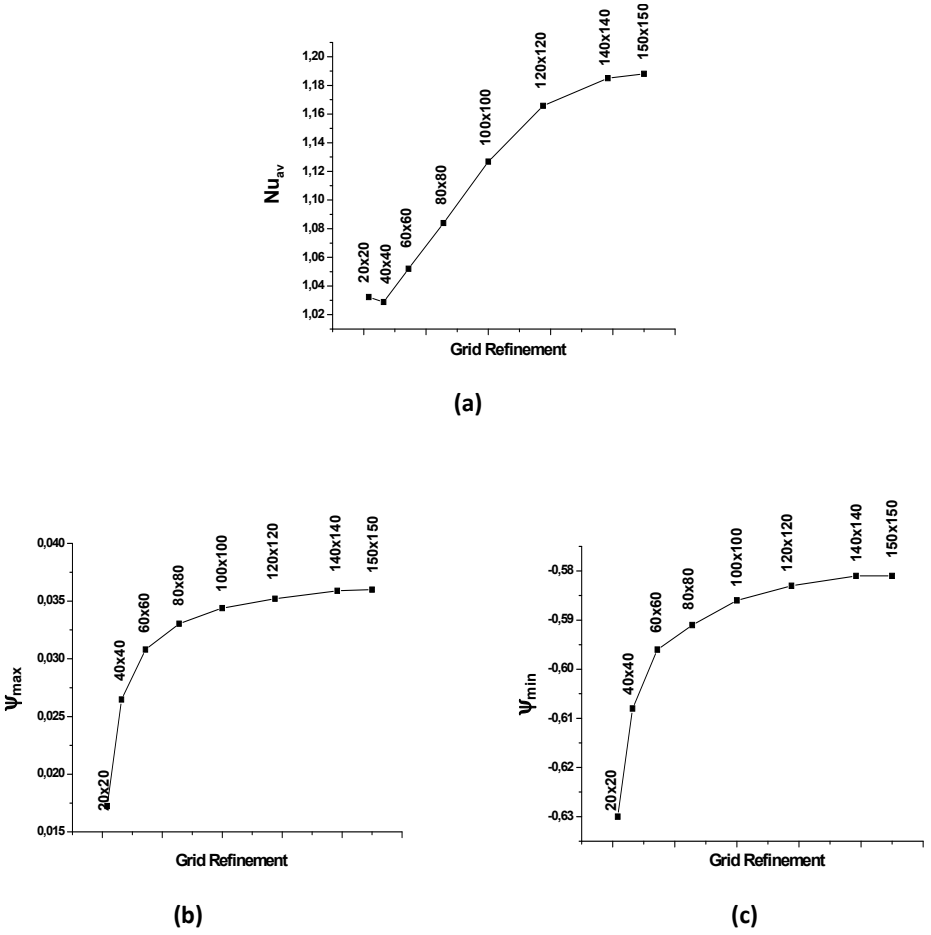

Figure 2: Convergence of the (a) average Nusselt number, (b) the maximum values of the stream function and (c) the minimum values of the stream function with grid refinement.

In order to obtain grid independent solution, a grid refinement study is performed for a square cavity (A= 1) with $Ha = 100$, $Ra = 20$ and $\phi = 0$. Fig. 2 shows the convergence of the average Nusselt number, Nu, at the heated surface, Fig. 2(a), the maximum$\psi_{\max}$, Fig. 2(b), and the minimum$\psi_{\min}$, Fig. 2(c), values of the stream

function with grid refinement. It is observed that grid independence is achieved with a 140×140 grid beyond which there is insignificant change inNu_{av}, $\psi_{\max}$ and $\psi_{\min}$. This grid resolution is therefore used for all subsequent computations.

4.1 Effects of varying the Rayleigh number on the flow field and the heat transfer

The resulting flow and temperature distributions are depicted in Fig. 3 where the convective flow streamlines for increasing values of the Rayleigh number. In this figure the presence of two cells flow patterns is noticed (Fig. 3a); one cell on the upper region of the cavity induced by of thermocapillary forces. From the streamlines one may also see that the size of the upper cell gradually decreases with the increase of the buoyancy parameter, *Ra*. This is possible, since an increase in the value of *Ra* will increase the dominancy of the buoyancy force over the magnetic field effect and the thermo-capillary force.

The corresponding effect of the increasing buoyancy forces on the isotherms is shown in Fig. 3b. From the figure we can ascertain that the increase in the buoyancy force causes the isotherms to deform significantly, and thin thermal boundary layers form near both the heated and cooled surfaces, which have enhanced the heat transfer rate as displayed in fig. 4.

4.2 Effects of varying the Hartmann number on the flow field and the heat transfer

Fig. 5a illustrates the effect of increasing values of the magnetic field parameter on the flow patterns when the magnetic field is applied horizontally ($\varphi = 0$). As the magnetic field increases forces, the convective flow in the cavern slows down and the vortex shifts to the right and upwards, thus, concentrating near the free surface of the melt. At Ha = 100, the Lorentz forces dominate and, as a result the distortion of the isotherms caused by the melt flow is very small, Fig. 5b. In the case of the horizontal magnetic field, it is seen that the streamlines in the upper part of the maps and the isotherms are equidistant. The main vortex shifts noticeably towards the upper surface, and the flow as a whole becomes multilayered. At Ha = 100 and 150, four and five vortices, respectively, are observed. From the value Ha=175, the structure of streamlines do not have a big change in their form, and remains the same for values of Ha> 200, fig. 6. It may be seen also, that the isotherms become more vertical and straighten out owing to the increase of the magnetic field strength, which is expected; since the magnetic field tend to weaken the flow, as observed above. The flow can be considered to be dominated by conduction phenomenon, as the convective motion has been totally inhibited. This effect can also be seen in Fig. 7.

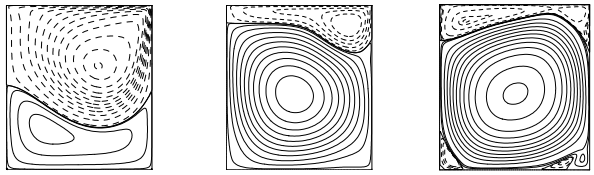

(a)

ψ_{max} =	0.121	1.941	2.217
ψ_{min} =	-1.018	-1.003	-0.719

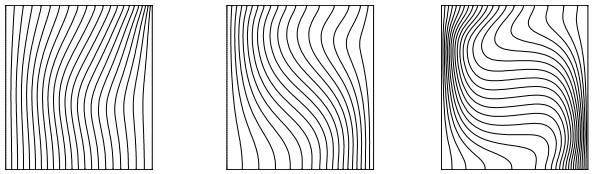

(b)

θ_{max} =	0.5	0.5	0.5
θ_{min} =	-0.5	-0.5	-0.5

Figure 3: Streamlines (top) and isotherms (bottom) for Ra= 10^3,10^4,10^5 while Ma=10^3, Ha=20 and $\varphi = 0$.

4.3 Effect of the direction of the external magnetic field on the flow and the temperature distribution

The effect of the direction of the external magnetic field, on the flow and the temperature distribution, is now discussed. Fig.8a, represents the streamlines obtained for $\varphi = 0, \pi/6, \pi/4, \pi/3$ and $\pi/2$ at Ra = 10^2, Ma= 10^3 and Ha= 10^2. As the direction of the external magnetic changes from horizontal to vertical, the flow rate in both the primary and the secondary cells decreases which causes an increase in the effect of the thermocapillary force and the flow becomes unicellular for$\phi = \pi/2$. The corresponding isotherms are depicted in Fig. 8b. In this figure, one can see that as the direction of the external magnetic field changes from 0 to $\pi/4$, the isotherms near the heated surface become parabolic; whereas a further change of the direction to $\pi/2$, that is when the magnetic field acts in the vertical direction, the isotherms near the heated and cold surface become more vertical and straighten out. All these because change in the direction reduces the flow rate in the cells which results in

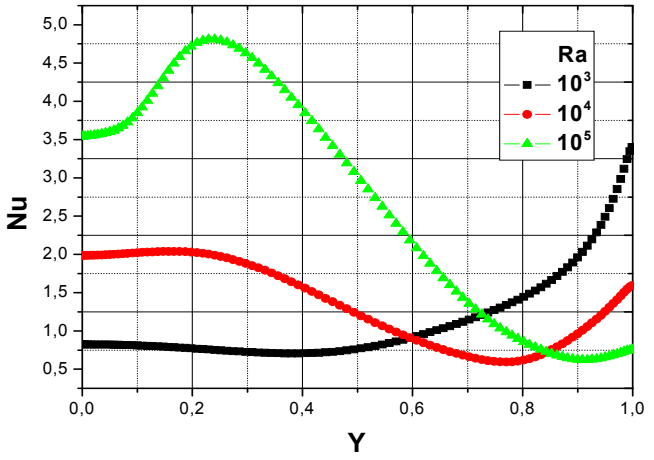

Figure 4: Numerical values of the local Nusselt number, Nu, on the right heated surface for different Ra and with $Ma = 10^3$, $Ha = 20$ and $\varphi = 0$.

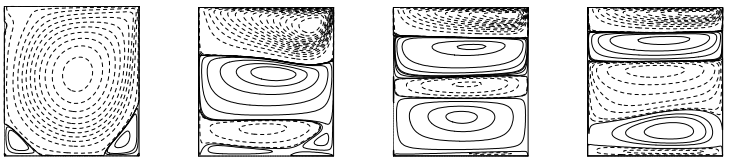

(a)

ψ_{max} =	0.046	0.039	0.034	0.029
ψ_{min} =	-2.121	-0.796	-0.599	-0.491

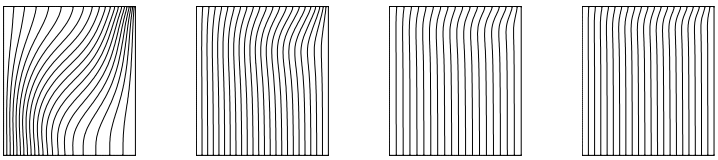

(b)

θ_{max} =	0.5	0.5	0.5	0.5
θ_{min} =	-0.5	-0.5	-0.5	-0.5

Figure 5: Streamlines (top) and isotherms (bottom) for Ha=0, 50,100,150 with Ma=10^3, Ra=20 and $\varphi = 0$.

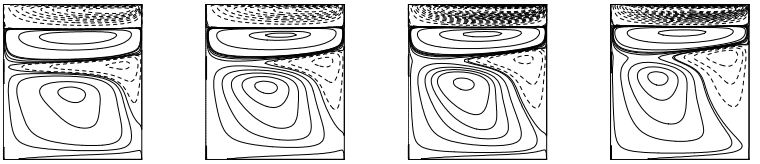

ψ_{max} =	0.026	0.023	0.021	0.019
ψ_{min} =	-2.121	-0.796	-0.599	-0.491

Figure 6: Streamlines for Ha=175, 200, 220,250 with Ma=10^3, Ra=20 and $\varphi = 0$.

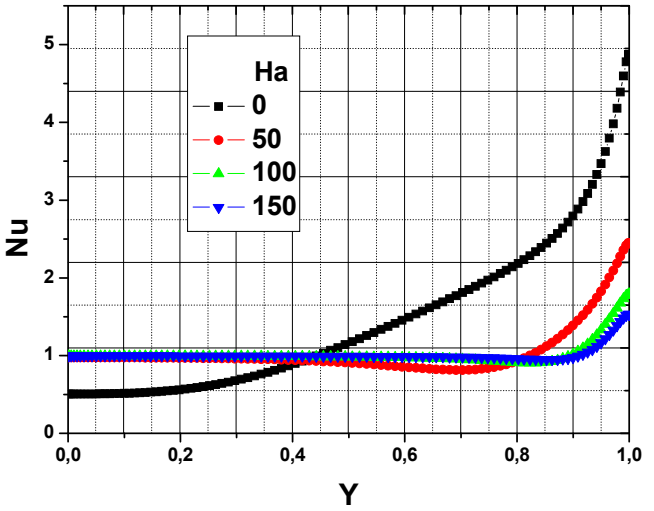

Figure 7: Numerical values of the local Nusselt number, Nu, on the right heated surface for different Ha with Ma=10^3, Ra=20 and $\varphi = 0$.

heat transfer rate reduction on the heated surface Fig. 9.

The variation of the average Nusselt number along the heated surface for different Hartmann number is shown in Fig. 10. It can be seen that the mean Nusselt number for Case Ra=10^5 is higher than that of Case Ra=20. Globally, the mean Nusselt number is a decreasing function of Hartmann number on nonisothermal wall. Differences between Nusselt numbers decrease with the increasing of Hartmann number due to increasing of domination of conduction mode of heat transfer,

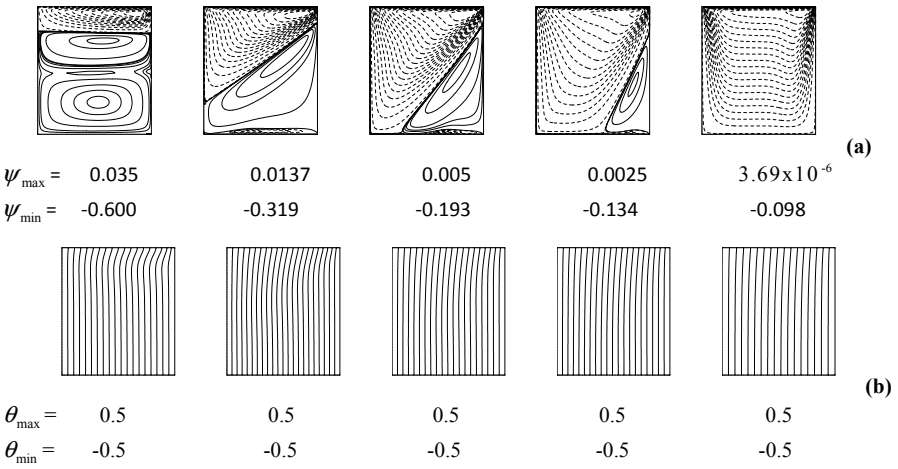

Figure 8: Streamlines (top) and isotherms (bottom) $\varphi = 0, \pi/6, \pi/4, \pi/3$ and $\pi/2$while Ra= 10^2, Ma= 10^3 and Ha= 10^2.

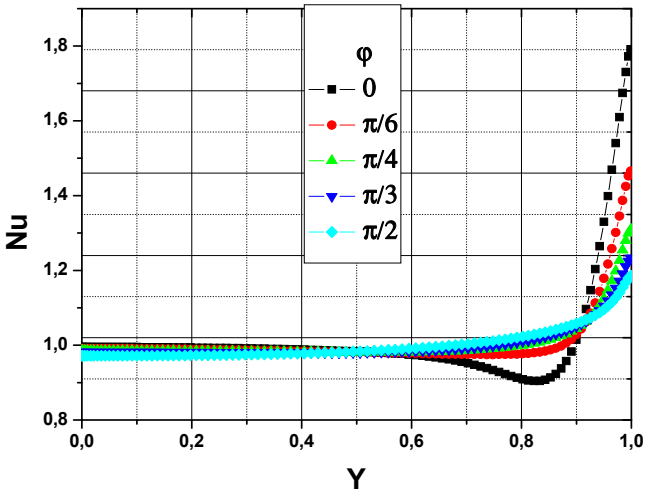

Figure 9: Numerical values of local Nusselt number, Nu, at the right heated surface for different φ at Ra= 10^2, Ma= 10^3 and Ha= 10^2.

due to the domination of the Lorentz forces. Variation of mean Nusselt numbers becomes constant for Ha> 100 in case that Ra=20, and for Ha> 150 in case that Ra> 10^5. This result is valid for all two cases considered for $\phi = 0$ or $\phi = \pi/2$.

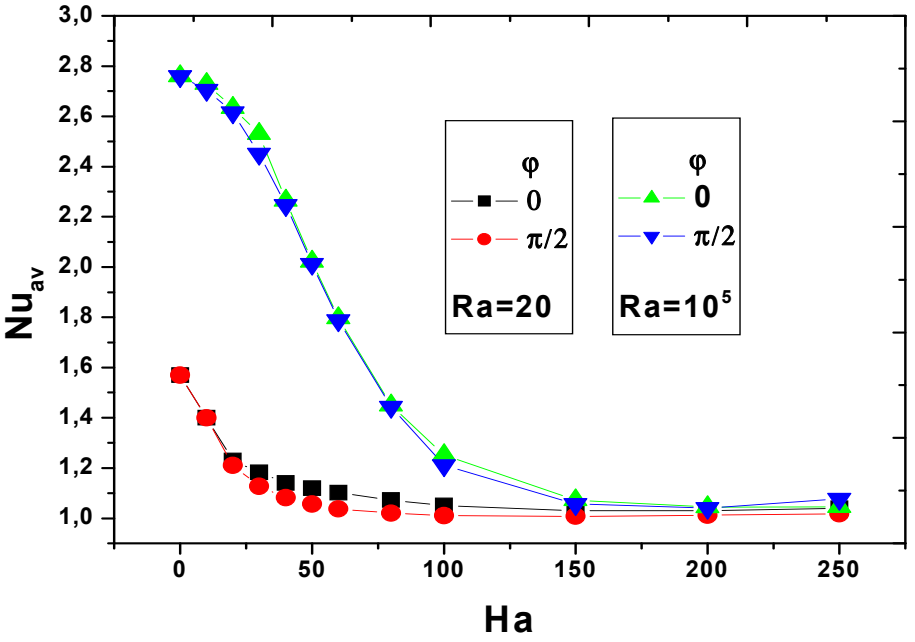

Figure 10: Variation of the average Nusselt number at the heated surface with Hartmann numberHa while Ra= (10^2,10^5), Ma= 10^3, Ha= 10^2 and $\phi = (0, \pi/2)$.

Fig. 11 depicts Variation of the average Nusselt number at the heated surface for differentϕ, for Ra= 20 and 10^5, the inclination angle ϕ of the magnetic field have an influence on Nu_{av}. As can be further seen from this figure, Nu_{av}tends to decrease when the magnetic field is inclined between ϕ = 0° and ϕ = 90°(and between ϕ = 180° and ϕ = 270°), and tends to increase when the magnetic field is inclined between ϕ = 90° and ϕ = 180°(and between ϕ = 270° and ϕ = 360°), and everything is in the case of the dominancy of the thermo-capillary force over the buoyancy force. A minimal value of Nu_{av}has been observed at ϕ = 180°(and ϕ=270). The physical mechanism behind this conclusion is that both the convective effect of the hot wall and the unstable effect of the cold wall are reduced by the inclination angle ϕ of magnetic field. But higher values of Nu_{av} are obtained in the case of ϕ = 0°, 180°(and 360°) .

In the case of the dominancy of the buoyancy force over the thermo-capillary force (Ra=10^5), we have a sinusoidal change of the average Nusselt number, Nu_{av}tends to decrease when the magnetic field is inclined between ϕ = 0° and ϕ = 30° and between ϕ = 150° and ϕ = 180°, and tends to increase when the magnetic field is inclined between ϕ = 30° and ϕ = 150°. The same change is observed in the other

semi-circle (between $\phi = 180°$ and $\phi = 360°$). A minimal value of Nu_{av}has been observed at $\phi = 30°$(and $\phi = 210°$) and a maximal value at $\phi = 150°$(and $\phi = 330°$).

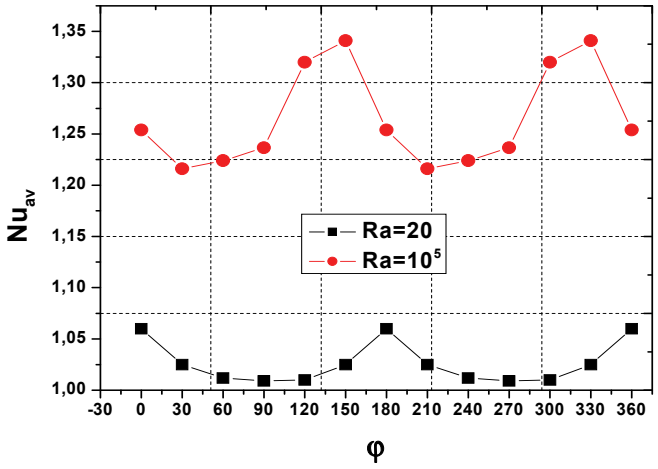

Figure 11: Numerical values of average Nusselt number, Nu_{av}, at the right heated surface for different ϕ while Ra= (10^2,10^5), Ma= 10^3 and Ha= 10^2.

5 Conclusions

The following conclusions may be drawn from the present investigations in which a laterally heated horizontal cavity with aspect ratio (height/width) =1 and Pr=0.015 subjected to both surface tension and buoyancy forces was considered:

In the case of the vertical magnetic field, both the isotherms and the streamlines are equidistant. The flow becomes unicellular; the flow can be considered to be dominated by conduction phenomena. In the case of the horizontal magnetic field, as the intensity of the magnetic field grows, the flow becomes multilayered with the main vortex shifted towards the free surface of the melt. The maximum absolute values of the stream function appear to be higher than the corresponding values obtained for the vertical field.

References

Achoubir, K.; Bennacer, R.; Cheddadi, A.; El Ganaoui, M.; Semma, E. (2008): Numerical Study of Thermosolutal Convection in Enclosures Used for Directional

Solidification (Bridgman Cavity), *FDMP: Fluid Dynamics & Materials Process*., Vol. 4, No. 3, pp. 199-210.

Armour, N.; Dost, S. (2009): Numerical and Experimental Study of Forced Mixing with Static Magnetic Field on SiGe System, *FDMP: Fluid Dynamics & Materials Process*., Vol. 5, No. 4, pp: 331-344.

Baumgartl, J.; Hubert, A.; Muller, G. (1993): The use of magnetohydrodynamic effects to investigate fluid flow in electrically conducting melts, *Phy. of Fluids*, Vol. A-5 (12), pp. 3280-3289.

Ben Hadid, H.; Henry, D.; Kaddeche, H. (1997): Numerical study of convection in the horizontal Bridgman configuration under the action of a constant magnetic field, Part 1: Two dimensional flow, *J. Fluid Mech.* Vol. 333, pp. 23–56.

Ben Hadid, H.; Roux, B. (1992): Buoyancy and thermocapillary driven flows in differentially heated cavities for low-Prandtl number fluids, *J. Fluid Mech*. Vol. 235, pp. 1.

Bucchignani, E. (2009): An Implicit Unsteady Finite Volume Formulation for Natural Convection in a Square Cavity, *FDMP: Fluid Dynamics & Materials Process*., Vol. 5, No. 1, pp. 37-60.

Djebali, R.; El Ganaoui, M.; Sammouda, H.; Bennacer, R., (2009): Some Benchmarks of a Side Wall Heated Cavity Using Lattice Boltzmann Approach, *FDMP: Fluid Dynamics & Materials Process*., Vol. 5, No. 3, 261-282.

Favier, J. J. (1990): *Recent advances in Bridgman growth modeling and fluid flow*, *J. Cryst. Growth* Vol. 99, pp. 18.

Gelfgat, A. YU.; Bar-Yoseph, P. Z. (2001): The effect of an external magnetic field on oscillatory instability of convective flows in a rectangular cavity, *Phys. Fluids*, Vol. 13(8), pp: 2269-2278.

Mechighel, F.; El Ganaoui, M.; Kadja, M.; Pateyron, B.; Dost, S. (2009): Numerical Simulation of Three Dimensional Low Prandtl Liquid Flow in a Parallelepiped Cavity Under an external Magnetic Field, *FDMP: Fluid Dynamics & Materials Process*., Vol. 5, No. 4, pp: 313-330.

Mezrhab, A.; Naji H.; (2009): Coupling of Lattice Boltzmann Equation and Finite Volume Method to Simulate Heat Transfer in a Square Cavity, *FDMP: Fluid Dynamics & Materials Process*., Vol. 5, No. 3, 283-296.

Ostrach, S. (1990): Low-gravity fluid flows, *Annu. Rev. Fluid Mech.* Vol. 14, pp. 313.

Ozoe, H.; Maruo, E. (1987): Magnetic and gravitational natural convection of melted silicon. Two-dimensional numerical computations for the rate of heat transfer, *JSME Int. J.,* Vol. 30, pp. 774–784.

Ozoe, H.; Okada, K. (1989): The effect of the direction of the external magnetic field on the three-dimensional natural convection in a cubical enclosure, *Int. J. Heat Mass Transfer,* Vol. 32, pp. 1939–1954.

Rudraiah, N.; Venkatachalappa, M.; Subbaraya, C. K. (1995): Combined surface tension and buoyancy-driven convection in a rectangular open cavity in the presence of a magnetic field, *Internat. J. Non-Linear Mech.* Vol. 30 (5), pp. 759.

Weiss, N. O. (1981): Convection in an imposed magnetic field. Part 1: The development of nonlinear convection, *J. Fluid Mech*., Vol.108, pp. 247–272.